Evaluation of vibration energy harvesting using a magnetostrictive iron cobalt/nickel-clad plate

doi: 10.1088/1361-665X/aaf9f2

Evaluation of Vibration Energy Harvesting Using a Magnetostrictive Iron-Cobalt/Nickel-Clad Plate

Zhenjun Yang[1], Hiroki Kurita[1], Ryuichi Onodera[2], Tsuyoki Tayama[2], Daiki Chiba[2] and Fumio Narita[1,a)]

[1]Department of Materials Processing, Graduate School of Engineering, Tohoku University, 6 Aoba-yama 6-6-02, Sendai 980-8579, Japan

[2]Research and Development Department, Tohoku Steel Co. Ltd., 23 Nishigaoka, Muratamachi, Shibatagun, Miyagi 989-1393, Japan

Abstract

The design of miniaturized, long-lasting power supplies for portable Internet of Things (IoT) equipment has been identified as a critical problem constraining further development of the IoT. A promising methodology is able to resolve the problem by harvesting dissipated energy such as vibration in the environment or in a system to form self-powered microsystems. In this work, the performance of vibration energy harvesting using a magnetostrictive iron-cobalt/nickel (FeCo/Ni)-clad plate cantilever was examined both theoretically and experimentally. The experimental results indicate that the output power of the FeCo/Ni-clad plate cantilever shows significant improvement in comparison to a single FeCo plate, as a result of the inverse magnetostrictive properties of the FeCo and Ni layers in response to tension or compression. Finite element analysis illustrates how the unidirectional and identical magnetic induction in the upper and lower sides (i.e. the FeCo and Ni layers) gives rise to this enhanced output. The analysis also demonstrates the cancellation of the positive and negative magnetic induction within the interior of the single FeCo plate. This study not only provides insights into the magnetic features of a FeCo/Ni-clad plate but also proposes a feasible method for realizing industrial applications.

Key words: magnetostrictive composite, simulation, iron-cobalt alloys, vibration, energy harvesting

a) narita@material.tohoku.ac.jp

1. Introduction

Magnetostrictive materials have been widely studied in recent years, not only in applications involving complicated sensors and actuators but also in energy-harvesting components [1-3]. In particular, following the rapid development of the Internet of things (IoT), these applications have been gaining a great deal of attention. The lack of availability of a miniaturized and long-lasting power supply is usually considered a primary issue hindering the further industrialization of portable IoT equipment. It seems that traditional batteries are clearly unsuitable to support the upcoming revolution in this field, not only owing to the difficulty in miniaturizing the volume of a battery cell for these microsystems, but also due to the inconvenience involved in recharging the battery. It is therefore imperative to develop effective and renewable alternatives. A promising methodology for resolving these problems is to harvest the dissipated energy (e.g. vibration) of the environment to form self-powered microsystems [4-7].

Vibration energy, as a renewable and clean energy source, is thought to be a promising solution for dealing with energy issues, especially using self-powered equipment with cyclical motion. In current techniques for harvesting vibration energy, two classes of materials are widely employed: piezoelectric and magnetostrictive materials. In general, most of the piezoelectric materials belong to a class of ceramic materials that are characterized by brittleness and low ductility [8,9]. In order to improve the power generation performance and the machining properties, a series of polymer materials such as PVDF have been introduced for the fabrication of ceramic/polymer composites. The applications of magnetostrictive materials have gradually begun to play an important role in harvesting vibration energy. This method is characterized by a relatively high output electric current compared to that of piezoelectric materials [10-12]. The main magnetostrictive materials are often classified into Terfenol-D and Galfenol alloys, and others. In addition, relevant research into other materials like Matglas and FeAl has also been reported [13]. In general, Terfenol-D has excellent magnetostriction but extreme brittleness. In order to resolve this problem, several researchers [14-16] have explored the fabrication of a polymer-matrix composite that is similar to piezo-polymer composites; however, the ductility has shown a limited increase at the expense of a significant decrease in the magnetostrictive properties. Furthermore, both the Terfenol-D and Galfenol alloys are typically expensive, due to the doping of rare element materials and the sophisticated processing required.

Iron cobalt has the benefit of significantly reducing the fabrication cost in comparison to other magnetostrictive materials. In this study, an easily producible iron-cobalt alloy (FeCo) is employed in the fabrication of a class of metal composites, and its performance is examined to reveal the excellent advantages of FeCo alloys as promising vibration energy components in comparison with some current commercial harvesters. This work describes the fabrication of a high-performance FeCo/Ni-clad plate cantilever to harvest vibration energy and compares it with a current commercial harvester. Together with a finite element simulation, it also provides insights into the mechanism responsible for energy conversion and finally offers the possibility of powering large-scale industrialized applications.

2. Formula and theoretical model

There is a general consensus that the generation of output power is associated with the domain rotation and/or domain wall movement caused by the uneven distribution of internal stress. However, it is often difficult to measure both the distribution of internal stress and the magnetic induction using conventional experimental methods. In order to understand the relevant mechanism, finite element analysis (FEA) is used here to simulate the variations in stress and magnetic induction of the FeCo/Ni clad plate cantilever under bending. The parameters employed (e.g. bias magnetic field, loading, etc.) match those used in the practical experiments.

The basic mathematical equations are listed below:

$$\sigma_{ji,j} = 0 \tag{1}$$

$$e_{ijk} H_{k,j} = 0, \qquad B_{i,i} = 0 \tag{2}$$

where σ_{ij}, H_i and B_i denote the components of the stress tensor, magnetic field intensity vector and magnetic induction vector, respectively. eijk is the permutation symbol, and the comma denotes partial differentiation with regard to the coordinates $x_i (i = 1, 2, 3)$. We use Cartesian tensor notation and the summation convention over repeated tensor indices. The constitutive equations are as follows:

$$\varepsilon_{ij} = s^{H}_{ijkl} \sigma_{kl} + d'_{kij} H_k \tag{3}$$

$$B_i = d'_{ikl}\,\sigma_{kl} + \mu_{ik} H_k \tag{4}$$

where ε_{ij} represents the components of the strain tensor, and s^H_{ijkl}, d'_{kij} and μ_{ik} are the elastic compliance, magnetoelastic constant and magnetic permeability of the constant magnetic field, respectively. These components confirm to the following symmetry correlation:

$$s^H_{ijkl} = s^H_{jikl} = s^H_{ijlk} = s^H_{klij}, \qquad d'_{kij} = d'_{kji}, \qquad \mu_{ij} = \mu_{ji} \tag{5}$$

The strain component can be denoted as

$$\varepsilon_{ij} = \frac{1}{2}(u_{j,i} + u_{i,j}) \tag{6}$$

where u_i is a component of the displacement vector. The magnetic field intensity vector is

$$H_i = \varphi_{,i} \tag{7}$$

where φ is the magnetic potential. Then, the constitutive equations (3) and (4) can be written as:

$$\begin{Bmatrix} \varepsilon_{11} \\ \varepsilon_{22} \\ \varepsilon_{33} \\ 2\varepsilon_{23} \\ 2\varepsilon_{31} \\ 2\varepsilon_{12} \end{Bmatrix} = \begin{bmatrix} s^H_{11} & s^H_{12} & s^H_{13} & 0 & 0 & 0 \\ s^H_{12} & s^H_{11} & s^H_{13} & 0 & 0 & 0 \\ s^H_{13} & s^H_{13} & s^H_{33} & 0 & 0 & 0 \\ 0 & 0 & 0 & s^H_{44} & 0 & 0 \\ 0 & 0 & 0 & 0 & s^H_{44} & 0 \\ 0 & 0 & 0 & 0 & 0 & s^H_{66} \end{bmatrix} \begin{Bmatrix} \sigma_{11} \\ \sigma_{22} \\ \sigma_{33} \\ \sigma_{23} \\ \sigma_{31} \\ \sigma_{12} \end{Bmatrix} + \begin{bmatrix} 0 & 0 & d'_{31} \\ 0 & 0 & d'_{31} \\ 0 & 0 & d'_{33} \\ 0 & d'_{15} & 0 \\ d'_{15} & 0 & 0 \\ 0 & 0 & 0 \end{bmatrix} \begin{Bmatrix} H_1 \\ H_2 \\ H_3 \end{Bmatrix} \tag{8}$$

$$\begin{Bmatrix} B_1 \\ B_2 \\ B_3 \end{Bmatrix} = \begin{bmatrix} 0 & 0 & 0 & 0 & d'_{15} & 0 \\ 0 & 0 & 0 & d'_{15} & 0 & 0 \\ d'_{31} & d'_{31} & d'_{33} & 0 & 0 & 0 \end{bmatrix} \begin{Bmatrix} \sigma_{11} \\ \sigma_{22} \\ \sigma_{33} \\ \sigma_{23} \\ \sigma_{31} \\ \sigma_{12} \end{Bmatrix} + \begin{bmatrix} \mu_{11} & 0 & 0 \\ 0 & \mu_{11} & 0 \\ 0 & 0 & \mu_{33} \end{bmatrix} \begin{Bmatrix} H_1 \\ H_2 \\ H_3 \end{Bmatrix} \tag{9}$$

where

$$\sigma_{23} = \sigma_{32}, \qquad \sigma_{31} = \sigma_{13}, \qquad \sigma_{12} = \sigma_{21} \tag{10}$$

$$\varepsilon_{23} = \varepsilon_{32}, \qquad \varepsilon_{31} = \varepsilon_{13}, \qquad \varepsilon_{12} = \varepsilon_{21} \tag{11}$$

$$s_{11}^H = s_{1111}^H = s_{2222}^H, \quad s_{12}^H = s_{1122}^H, \quad s_{13}^H = s_{1133}^H = s_{2233}^H, \quad s_{33}^H = s_{3333}^H,$$
$$s_{44}^H = 4s_{2323}^H = 4s_{3131}^H, \quad s_{66}^H = 4s_{1212}^H = 2\left(s_{11}^H - s_{12}^H\right) \tag{12}$$

$$d'_{15} = 2d'_{131} = 2d'_{223}, \quad d'_{31} = d'_{311} = d'_{322}, \quad d'_{33} = d'_{333} \tag{13}$$

A three-dimensional finite element model is utilized to analyze the stress distributions and magnetic flux variation for the FeCo alloys. The coordinate axes x_1 and x_2 are chosen for the x and y axes, respectively, and thus the $z = x_3$ axis indicates the axis that can be easily magnetized. In practical experiments, a magnetic bias field is always along the length direction (easy axis), and the transverse (31) magnetostrictive deformation mode is dominant. Hence, the constants d'_{15}, d'_{31} and d'_{33} are:

$$d'_{15} = d^m_{15}$$
$$d'_{31} = d^m_{31} \tag{14}$$
$$d'_{33} = d^m_{33} + m_{33}H_3$$

where d^m_{15}, d^m_{31} and d^m_{33} are the piezo-magnetic constants, and m_{33} is the second-order magnetoelastic constant [17]. The constant m_{33} is 1.23×10^{-14} m^2/A^2. The constitutive equations for the magnetostrictive materials are mathematically consistent with those for piezoelectric materials. The commercial package ANSYS was used in this simulation, as it allows for coupled-field solid, acoustic fluid and infinite acoustic elements. Our previous works [18, 19] have verified the scheme presented above and have shown that the obtained results are of general applicability. The relevant properties of FeCo and Ni alloys used in the calculation for the FEA are given in Table 1 [20].

3. Experiment

In this study, the forged FeCo alloys were treated by rolling and then joined with cold-rolled nickel alloy, using the hot pressing bonding method to fabricate the FeCo/Ni-clad plate. In more detail, the raw materials were initially melted in a furnace, and then the melted ingot was shaped into crude slabs by forging, before undergoing hot and cold rolling. Finally, the FeCo and Ni layers were bonded using thermal diffusion bonding. More details of this process can be found in our previous work on an FeCo/Fe-clad plate [11]. During this process, a pre-stress was introduced to the clad plate in order

to facilitate the movement of the domain wall and/or rotation of the domain. This effect has been reported in previous works [20-22]. Following this, the clad plate was processed into the experimental specimen with dimensions of approximately 70 mm × 50 mm × 1 mm. A single FeCo plate was also cut to identical dimensions for comparison. It should be noted here that the power generation properties of a commercial piezoelectric bimorph cantilever (THRIVEK7520BS3; Thrive Co., Ltd., Japan) were also examined in order to compare the feasibility of industrialization for this high-performance FeCo-related magnetostrictive harvester.

The specific physical assembly and schematic for vibration energy harvesting is shown in Fig. 1. The upper part of the image shows the measurement of the output power generation for the FeCo/Ni or FeCo cantilever in Fig. 1(a). A proof mass was positioned at the free end of the cantilever and an outside load resistance (66 kΩ) was connected with the pickup coil. A functional generator was employed to provide a sinusoidal signal that was then transmitted to an amplifier to drive a bending vibration shaker. The input frequency was in the range 40 Hz to 60 Hz, and the amplitude was adjustable depending upon the acceleration a = 0.1–1.5 g. The magnetostrictive cantilever was magnetized using a magnet (i.e. a magnetic bias field B_0) positioned at the clamped end of the cantilever. The cantilever was enclosed by the coil windings (6.4×10^4 turns), and the effective volume for generation is approximately 200 mm^3. The output voltage due to the bending vibration was harvested by a pickup coil with an intrinsic resistance of approximately 66 kΩ, which is connected to an oscilloscope. The single FeCo plate cantilever was prepared using an identical method. The physical assembly for harvesting vibration energy for the piezoelectric bimorph cantilever with a capacitance of 110 nF (THRIVE K7520BS3; Thrive Co., Ltd., Japan) is shown in the lower part of Fig.1 (a). The practical generating volume of the piezoelectric bimorph is about 332 mm^3. To examine the effects of residual stress on domain rotation and/or domain wall movement, the measurement of residual stress on each layer of the FeCo/Ni clad plate was carried out using a setup of μ-X360s (Pulstec Industrial Co., Ltd., Japan).

4. Results and discussion

The input frequency has a vital effect on power generation output, and it is therefore necessary to examine the resonance frequency to identify the optimal frequency. In this work, the correlation

between the input frequency and the output power/voltage was measured in the range 40 to 60 Hz. The resonance frequency of the setup for the FeCo/Ni clad plate cantilever was about 50 Hz. The input frequency to the single FeCo plate cantilever was adjusted to match this output performance at the same frequency (50 Hz). Fig. 2 shows comparisons of the output power and voltage for the two different cantilevers (FeCo/Ni and single FeCo) within a specific range of input frequency. It is obvious that both the output power and voltage of the FeCo/Ni clad plate cantilever are significantly greater than those of the single FeCo plate cantilever. The maximum values of output power and voltage for the FeCo/Ni clad plate cantilever are 1.68 mW and 10.52 V, respectively; these data are greater than those for the single FeCo plate by factors of approximately 12 and 3.5, respectively. It is easy to see that the usable bandwidth of the FeCo/Ni clad plate cantilever is also dramatically broader than that of the single FeCo plate cantilever. As a consequence, it is reasonable to believe that this bonding method for preparing FeCo/Ni alloys has the benefits of increasing the serviceable range of the vibration energy harvester.

The output voltages for the FeCo/Ni clad plate cantilever and the single FeCo plate cantilever exhibit different features, as shown in Fig. 3. The maximum output voltage for the single FeCo plate is only about 2.8 V at a load resistance of 66 KΩ, an acceleration of 0.25 g and a frequency of 50 Hz. In contrast, that of FeCo/Ni clad plate cantilever is significantly increased. In addition to the maximum value, the output cycle times for these two specimens show obvious differences; the time for one cycle of the FeCo/Ni clad plate cantilever is twice that of the single FeCo plate cantilever. The reason for this is related to the distribution of magnetic induction within the interior of these specimens in response to the bending vibration. For the single FeCo plate cantilever, the magnetic domain induced by bending aligns in a reverse orientation along with the neutral plane, leading to a cancellation of the magnetic induction density. This effect is very noticeable under the maximum deflection during the bending deformation, and the output voltage of the single FeCo plate cantilever at this position is therefore close to 0 V (see the dotted line in Fig. 3). In contrast, there is no cancellation of the magnetic induction density for the FeCo/Ni-clad plate cantilever during the bending deformation; instead, the FeCo and Ni layers can enhance the vibration-induced variation in magnetic induction density for each other, due to their different magnetostrictive properties. This is evident when observing the output voltage for the FeCo/Ni-clad plate cantilever at maximum deflection. Although the upper and lower sides (i.e. the FeCo and Ni layers) are subjected to differing stresses due to bending, the entire clad plate is able to maintain a unidirectional magnetic induction owing to the counter-

magnetostriction of FeCo and Ni in response to the compressive and tensile bending stress. To enable a better understanding of this, the magnetic induction vector is shown in the right inset of Fig. 3.

An ANSYS simulation was used to determine the reason for the difference between the FeCo/Ni and single FeCo cantilevers. Fig. 4 shows the variations in the magnetic induction density and normal stress along the direction of thickness (i.e. *y*-axis) for the FeCo/Ni and single FeCo cantilevers at a chosen point ($x = z = 0$ mm here). The model is shown in Fig. 4(a). The distributions of the magnetic induction density for these two cantilevers in response to the same bending load are significantly different, especially along the neutral plane (i.e. the middle of the *y*-axis) at the maximum deflection (see Fig. 4(b)). In the single FeCo cantilever, due to the tension and compression resulting from bending, the directions of the magnetic induction density in the upper and lower layers are opposite. The total magnetic induction density within the coil windings at maximum deflection hardly varies as a result of the cancellation of the upper and lower magnetic induction densities. In contrast, the magnetic induction densities for the two layers (i.e. FeCo and Ni) of the FeCo/Ni-clad plate cantilever exhibit an approximately symmetrical distribution due to the inverse magnetostrictive properties of the FeCo and Ni alloys. As a consequence, the total magnetic induction density within the coil windings is superposed, generating greater power at the maximum deflection. In addition, according to the normal stress distribution shown in the Fig. 4(c), these two cantilevers have similar curves. It is therefore clear that the distribution characteristics of the magnetic induction densities in the interior of these two cantilevers are the vital factors responsible for the differences in power generation. An interesting phenomenon arises in that the curve of FeCo/Ni peaks at the interface due to the particular boundary conditions used, unlike that of the single FeCo alloy. Across the interface, the continuity of the tangential component of the magnetic field intensity vector H_t can be expressed as

$$H_t^+ = H_t^-$$

and the continuity of the normal component of the magnetic induction vector B_n is

$$B_n^+ = B_n^-$$

where the superscripts + and – denote the upper and lower interfaces of the FeCo and Ni alloys. In contrast, there is no relevant interface within the single FeCo cantilever, so the value of the magnetic induction density (B_z) at the corresponding position is therefore zero. On the other hand, since the

FeCo/Ni plate is prepared by the hot pressing bonding method, residual stress inevitably exists, which has an effect on the performance of energy harvesting. The residual stresses in each layer of the FeCo/Ni plate were therefore measured (see Table 2). Both of these layers (FeCo and Ni) undergo tensile stress, and as a result, the magnetic domain is susceptible to generate rotation or movement.

In order to evaluate the potential industrial applications of harvesting vibration energy using this novel FeCo-related composite, a comparison was carried out of the output power densities (PD) of the FeCo/Ni clad plate cantilever and the piezoelectric bimorph cantilever (Fig. 5). A load mass was employed to tune the resonance frequency of the piezoelectric bimorph cantilever to ensure the effectiveness of the comparison at the same frequency of 50 Hz. In Fig. 5(a), the output power density is clearly proportional to both the input acceleration and the load resistance. The variation in the output power density for the piezoelectric bimorph shown in Fig. 5(b) is analogous to that of the FeCo/Ni-clad plate cantilever; however, the energy-harvesting performance of the FeCo/Ni cantilever is far greater than that of the commercial piezoelectric bimorph. In addition, several slight disparities can also be found: the FeCo/Ni clad plate cantilever has a relatively broad usable range for the variation in both the load resistance and the acceleration. In addition to this advantage, the FeCo/Ni-clad plate cantilever is more sensitive to changes in the load resistance and input acceleration. In order to facilitate the determination of optimal parameters, an evaluative criterion is used for the normalized PD (NPD $=$ PD$/a$), and the effects of frequency and load resistance are omitted here. These features are illustrated in Fig. 6. From the NPD metrics, it is easy to observe a correlation between the output power and input acceleration. The NPD of the FeCo/Ni-clad plate cantilever peaks at an acceleration of 0.3 g, and then shows a downward tendency. In contrast, the NPD of the piezoelectric bimorph cantilever increases with an increase in input acceleration. Additionally, the NPD value for the piezoelectric bimorph is much lower than that of the FeCo/Ni cantilever. These findings indicate that the FeCo/Ni-clad plate cantilever has a promising capacity for application at a relatively low acceleration, and outperforms even some commercial products.

5. Conclusion

A promising novel FeCo/Ni-clad plate cantilever for harvesting vibration energy was proposed in this work. In order to evaluate the capacity for energy conversion of the FeCo/Ni-clad plate cantilever, a

single FeCo plate cantilever and a commercial piezoelectric bimorph cantilever were also examined. The results reveal that the output power and the voltage for the FeCo/Ni-clad plate cantilever are greater than those of the single FeCo cantilever by factors of approximately 12 and 3.5, respectively. Furthermore, the output cycle time of the FeCo/Ni-clad plate cantilever is significantly broadened compared to the single FeCo plate cantilever, due to the counter-response of the magnetostriction with respect to bending vibration. An FEA demonstrates that the different magnetostrictive properties of FeCo and Ni alloys are responsible for the superposition of output power generation. In contrast, the interior cancellation of the magnetic induction in the single FeCo plate leads to the phenomenon of no output voltage below maximum deflection. The output of the FeCo/Ni-clad plate cantilever is also proportional to the load resistance, and the capacity for output generation is far greater than that of the commercial piezoelectric bimorph cantilever. In addition to this, it is obvious that the FeCo/Ni-clad plate cantilever has a highly usable wideband frequency for multiple applications. Furthermore, measurement of the NPD indicates that the FeCo/Ni-clad plate cantilever is able to harvest the vibration energy at a relatively low acceleration. In conclusion, the FeCo/Ni clad plate cantilever shows excellent cost-effectiveness and good magnetic properties; as a result, this class of FeCo-related composites can be widely employed not only in vibration energy harvesters but also in high-sensitivity sensors or actuators.

References

[1] Tang C P and Lu C J 2016 *J. Alloy Compd*. **686** 723-726

[2] Deng Z X and Dapino M J 2017 *Smart Mater. Struct.* **26** 103001

[3] Narita F and Fox M 2018 *Adv. Eng. Mater.* **20** 1700743

[4] Mohammadi S and Esfandiari A 2015 *Energy* **81** 519-525

[5] Jafari H, Ghodsi A, Azizi S and Ghazavi M R 2017 *Energy* **124** 1-8

[6] Deng Z X and Dapino M J 2017 *Smart Mater. Struct*. **26** 055027

[7] Lekha C S C, Kumar A S, Vivek S, Rasi U P M, Saravanan K V, Nandakumar K and Nair S S 2017 *Nanotechnology* 28 055402

[8] Wang Y Z and Atulasimha J 2012 *Smart Mater. Struct*. **21** 085023

[9] Chen L, Li P, Wen Y and Zhu Y 2015 *Compos. Struct.* **119** 685-692

[10] Yoffe A and Shilo D 2017 *Smart Mater. Struct*. **26** 065007

[11] Yang Z J, Nakajima K, Onodera R, Tayama T, Chiba D and Narita F 2018 *Appl. Phys. Lett.* **112** 073902

[12] Qian F, Zhou W L, Kaluvan S, Zhang H F and Zuo L 2018 *Smart Mater. Struct.* **27** 045018

[13] Han Y J, Wang H, Zhang T L, He Y K and Jiang C B 2018 *Appl. Phys. Lett* .**112** 082402

[14] Deng Z X 2017 *J. Appl. Phys.* **122** 043901

[15] Adelsberg N, Weber Y, Yoffe A and Shilo D 2017 *Smart Mater. Struct*. **26** 065013

[16] Yan B P, Zhang C M and Li L Y 2018 *AIP Adv.* **8** 056730

[17] Jia Z, Liu W, Zhang Y, Wang F, Guo D 2006 *Sens. Actuators A Phys.* **128** 158-164

[18] Shindo Y, Mori K, Narita F 2010 *Acta Mechanica* **212** 253-261

[19] Yang Z J, Kurita H, Takeuchi H, Katabira K, Narita F *Adv. Eng. Mater*. in press.

[20] Narita F and Katabira K 2017 *Mater. Trans*. **58** 302-304

[21] Narita F 2017 *Adv. Eng. Mater.* **19** 1600586

[22] Katabira K, Yoshida Y, Masuda A, Watanabe A and Narita F 2018 *Materials* **11** 406

Table 1. Material properties of the FeCo and Ni alloys

Materials	Elastic compliance ($\times 10^{-12}$ m^2 N^{-1})						Piezomagnetic constant ($\times 10^{-12}$ m^2 A^{-1})			Relative permeability	
	s_{11}^H	s_{33}^H	s_{44}^H	s_{66}^H	s_{12}^H	s_{13}^H	d_{31}	d_{33}	d_{15}	μ_{11}	μ_{33}
FeCo	5.5	5.5	14.3	14.3	−1.65	−1.65	−60.3	125	318	100	100
Ni	5	5	13.1	13.1	−1.55	−1.55	35.5	−73.6	−187.2	200	200

Table 2. Comparison of residual stresses for each layer of the FeCo/Ni-clad plate cantilever

Layer	Residual stress (MPa)
FeCo	104.5
Ni	44.5

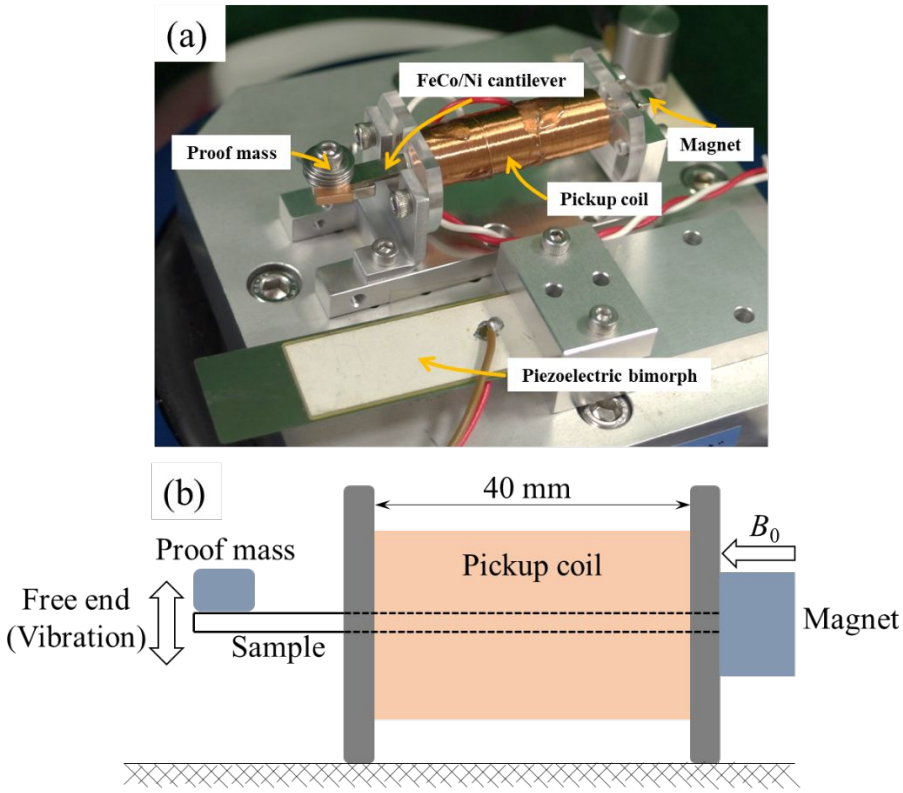

Fig. 1 (a) Physical assembly and (b) schematic diagram for harvesting vibration energy

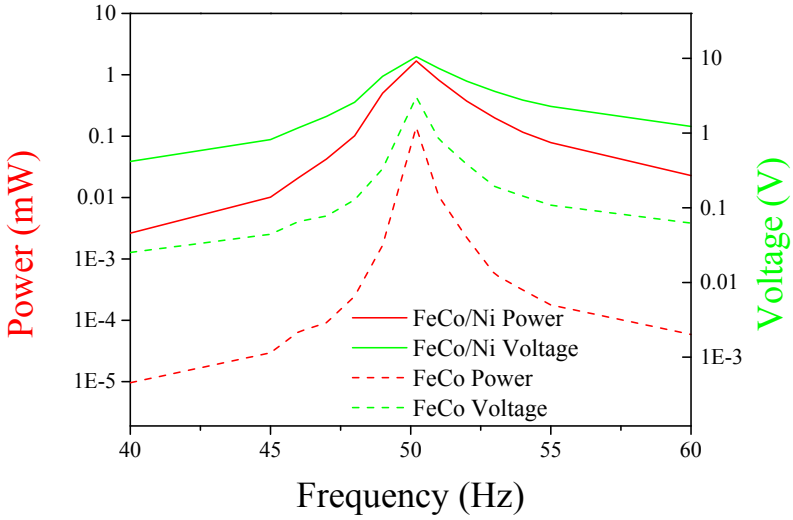

Fig. 2 Comparison of the output power and voltage as a function of the frequency of the FeCo/Ni and signal FeCo cantilevers at a load resistance of 66 kΩ and an amplitude of 0.05 mm

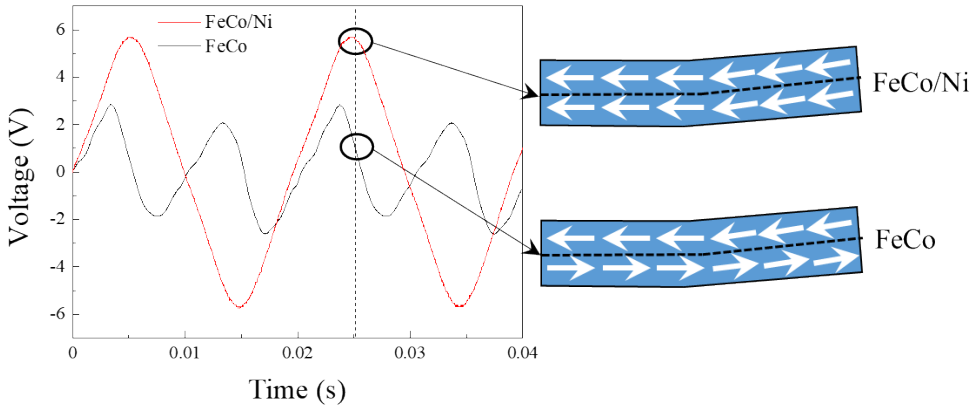

Fig. 3 Comparison of the output voltage for the FeCo/Ni and signal FeCo cantilevers at a load resistance of 66 kΩ, an amplitude of 0.05 mm, an acceleration of 0.25 g and a frequency of 50 Hz; the right insets show the direction of the magnetic induction vector under maximum deflection

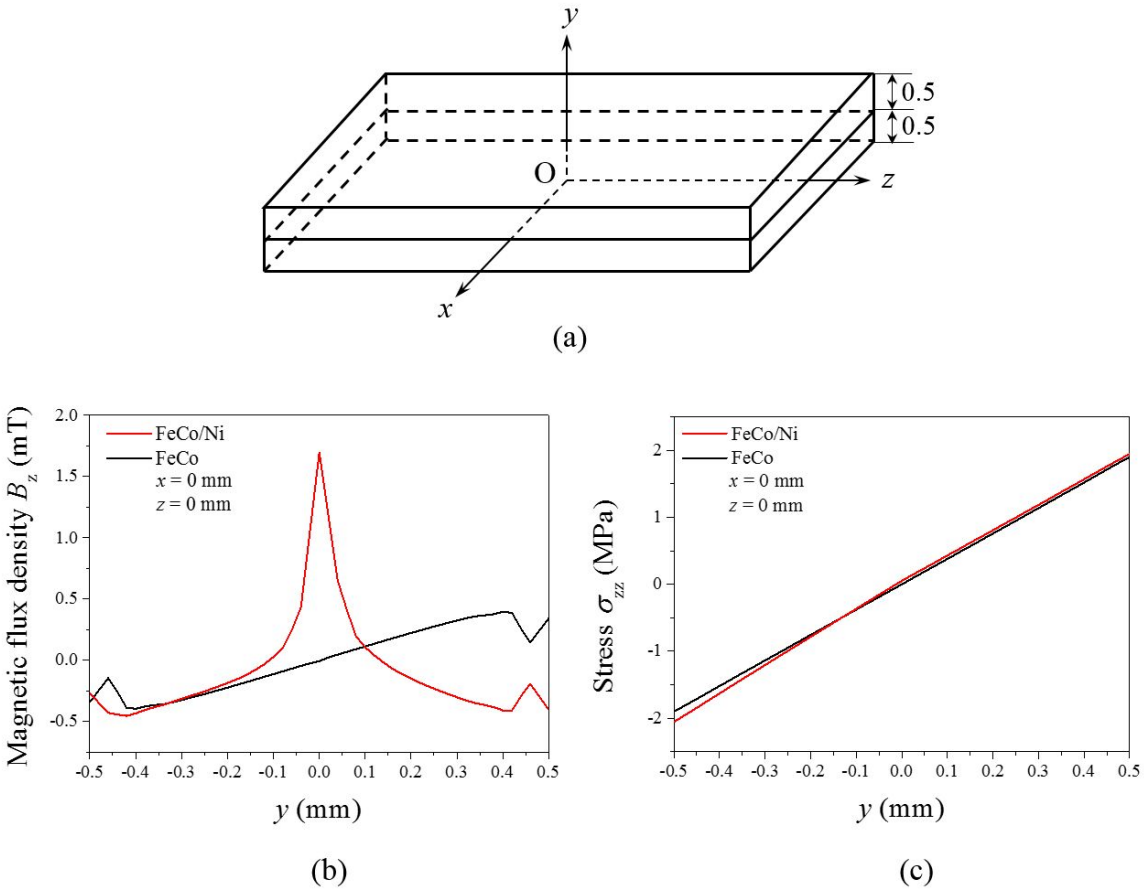

Fig. 4 (a) Schematic for the ANSYS model; variations of the (b) magnetic induction density and (c) normal stress for the FeCo and FeCo/Ni cantilevers along the direction of thickness

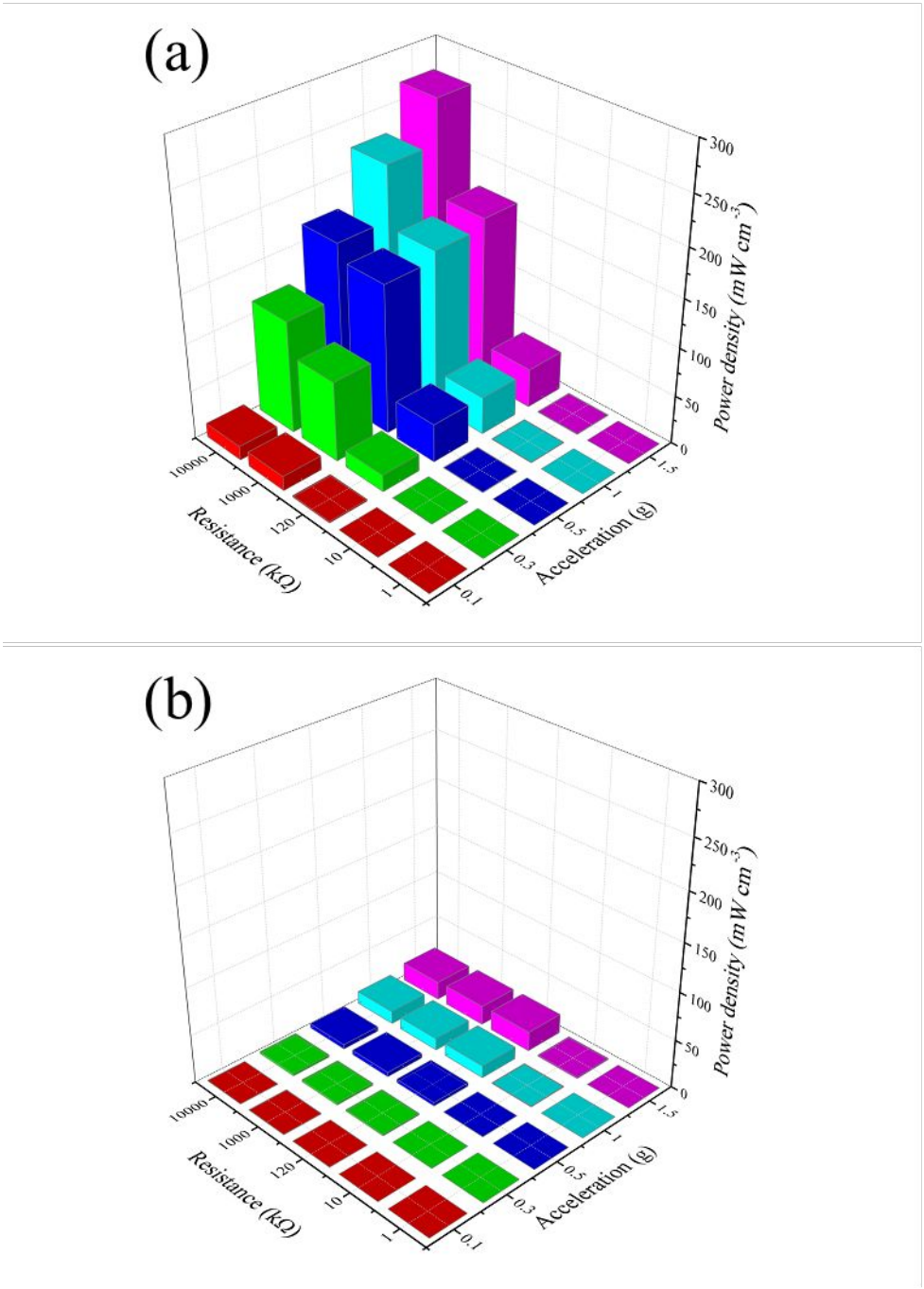

Fig. 5 Power density of the (a) FeCo/Ni and (b) piezoelectric bimorph cantilevers at different load resistances and accelerations, at a frequency of 50 Hz

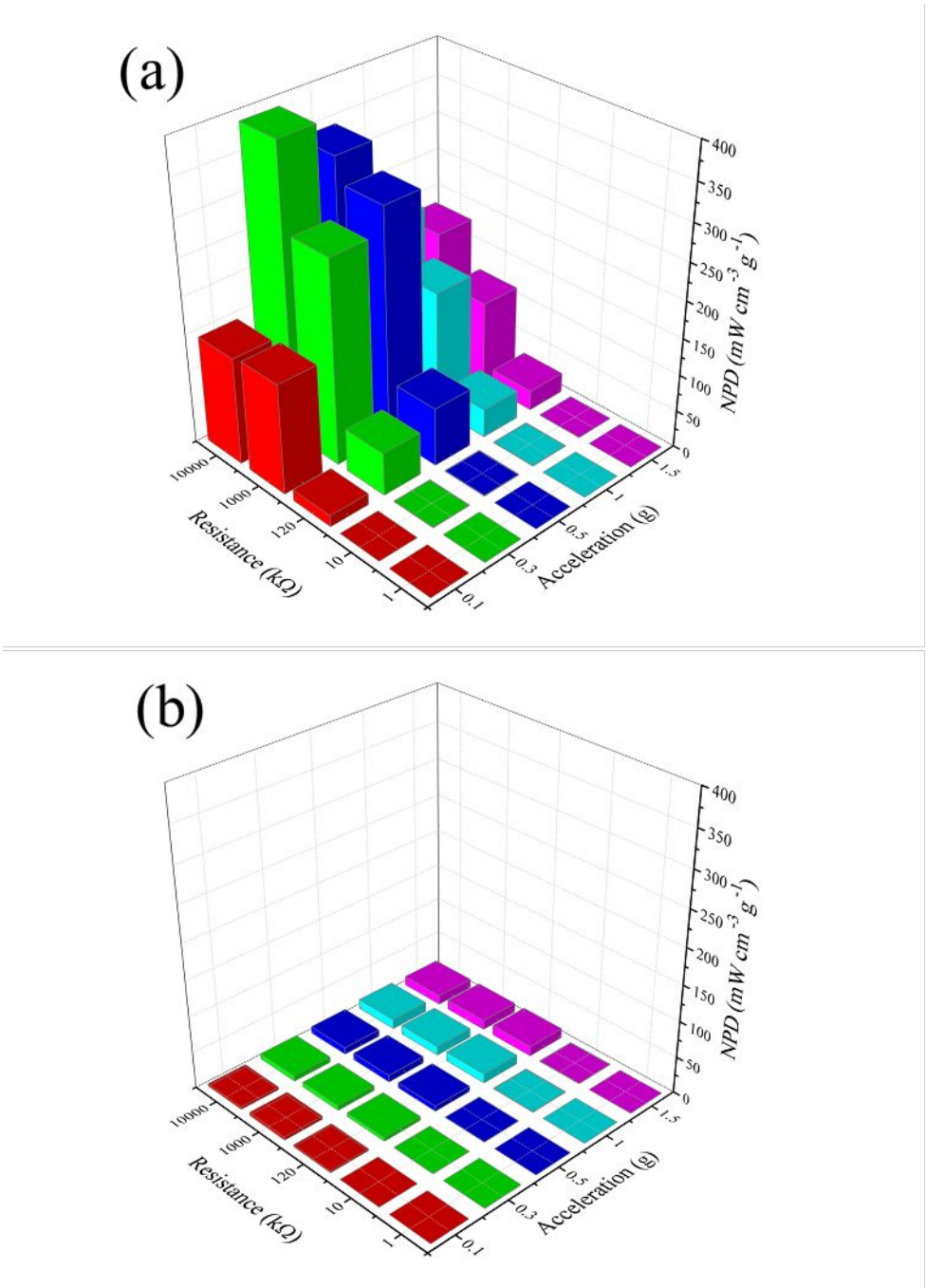

Fig. 6 Normalized power density of the (a) FeCo/Ni and (b) piezoelectric bimorph cantilevers at different load resistances and accelerations, at a frequency of 50 Hz